Angewandte Chemie
Eine Zeitschrift der Gesellschaft Deutscher Chemiker

Supporting Information

Conductive Fused Porphyrin Tapes on Sensitive Substrates by a Chemical Vapor Deposition Approach

*Giuseppe Bengasi, Kamal Baba, Gilles Frache, Jessica Desport, Paul Gratia, Katja Heinze, and Nicolas D. Boscher**

anie_201814034_sm_miscellaneous_information.pdf

Author Contributions

G.B. Data curation: Lead; Formal analysis: Lead; Writing—original draft: Lead; Writing—review & editing: Lead
K.B. Data curation: Supporting; Formal analysis: Supporting; Writing—original draft: Supporting; Writing—review & editing: Supporting
G.F. Data curation: Supporting; Formal analysis: Supporting; Methodology: Supporting; Validation: Supporting; Writing—review & editing: Supporting
J.D. Data curation: Supporting; Formal analysis: Supporting; Methodology: Supporting; Writing—review & editing: Supporting
P.G. Data curation: Supporting; Formal analysis: Supporting; Methodology: Supporting; Writing—review & editing: Supporting
K.H. Data curation: Supporting; Methodology: Supporting; Supervision: Supporting; Validation: Supporting; Writing—review & editing: Supporting
N.B. Conceptualization: Lead; Data curation: Supporting; Formal analysis: Supporting; Funding acquisition: Lead; Investigation: Equal; Methodology: Lead; Project administration: Lead; Resources: Lead; Supervision: Lead; Validation: Lead; Writing—original draft: Supporting; Writing—review & editing: Equal.

Table of Contents

Experimental Procedures

Oxidative Chemical Vapor Deposition

The oCVD experiments described in this paper were performed in a custom-built oCVD reactor (Figure 1). The reactor body is a stainless steel cube of 41 cm on each side (Kurt J. Lesker Co.) equipped with a dry scroll pump (Varian) and a turbomolecular pump (Agilent) to achieve high vacuum. A butterfly type throttling valve (VAT) and a microleak valve fed with argon (Air Liquide, 99.999 %) were used to maintain the pressure to 10^{-3} mbar for all the deposition experiments. Pressure was monitored by means of a baratron vacuum gauge (MKS). At the bottom of the chamber are two low temperature evaporation (LTE) point sources (Kurt J. Lesker Co.) to supply the porphyrin and the oxidant to a temperature-controlled substrate holder (Thermocoax) located approximately 20 cm above. For the preparation of the oCVD NiDPP coating, the evaporators were loaded with 10 mg of nickel(II) 5,15-(diphenyl)porphyrin (NiDPP) and 150 mg of $FeCl_3$ and heated to 250 °C and 170 °C, respectively. For the preparation of the oCVD NiDD*t*-BuPP coating, the evaporators were loaded with 10 mg of nickel(II) 5,15-bis(di-3,5-tert-butylphenyl) porphyrin (NiDDt-BPP) and 150 mg of $FeCl_3$ and heated to 260 °C and 150 °C, respectively. Microscope glass slides, silicon wafers, printer paper sheets and organic field effect transistor chips (OFET) (Fraunhofer) were used as substrates. The substrate holder temperature was maintained at 130 °C and the deposition time was 30 minutes when coating the microscope glass slides, silicon wafers and OFET chips. The substrate holder temperature was maintained at 60 °C and the deposition time was 30 minutes when coating the printer paper sheets.

Materials and Reagents

NiDPP was prepared by metalation of 5,15-(diphenyl)porphyrin H_2DPP (PorphyChem, 98 %) with $Ni(OAc)_2 \times 4H_2O$.[1] NiDD*t*-BuPP was purchase from (PorphyChem, 98 %) and used as supply. The oxidant, iron(III) chloride ($FeCl_3$), was obtained from Sigma-Aldrich and used without further purification (97 %).

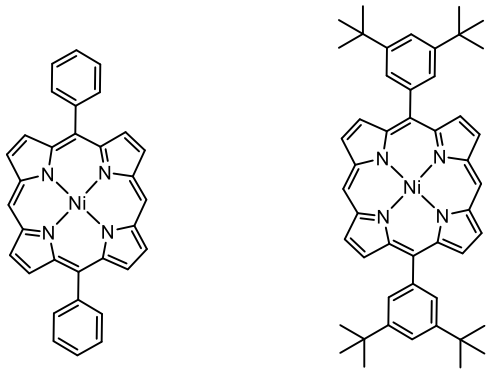

NiDPP NiDD*t*-BuPP

Scheme S1. Chemical structure for NiDPP and NiDD*t*-BuPP

Characterisation Methods

The thin films thicknesses were measured using a KLA-Tencor P-17 Stylus profiler.

The optical absorbance was measured in the range of 250–2000 nm using an UV-Vis-NIR spectrophotometer (Perkin Elmer, Lambda 950) with a 150 mm diameter integrating sphere. The absorption spectra were recorded directly on the glass substrates before and after rinsing the glass with dichloromethane (DCM), tetrahydrofuran (THF) and acetone. The coated glass substrates were rinsed by washing repeatedly with about 4 ml of solvent. The UV-Vis-NIR spectrum of the soluble phase of the coating in acetone or DCM was measured in quartz cuvettes of 3.5 mL and 1 cm light path.

X-ray photoelectron spectroscopy (XPS) analyses were performed on a Kratos Axis Ultra DLD instrument using a monochromatic Al Kα X-ray source ($\hbar\upsilon$ = 1486.6 eV) at a power of 105 W. Charge calibration was accomplished by fixing the binding energy of carbon (C 1s) to 285.0 eV.

Laser desorption/ionization high-resolution mass spectra (LDI-HRMS) measurements were performed on an AP-MALDI UHR ion source from MassTech, Inc. coupled to an LTQ/Orbitrap Elite from Thermo Scientific. oCVD coated Si wafers were directly placed on the sample holder, adjusting the working distance to optimum. In source fragmentation (E = 70 V) was used to prevent the formation of clusters.

Gel permeation chromatography was performed using an Ultimate 3000 apparatus from ThermoFicher, equipped with an ERC differential refractive index detector and a UV detector. Samples were dissolved in tetrahydrofuran (THF) containing 1 vol.% of pyridine, as described elsewhere[2] and filtered over a 0.25 µm pore size membrane prior to injection. Flow rate was set to 1 $mL \cdot min^{-1}$. A mesopore column 3 µm (300 × 7.5 mm) from Agilent Technologies was used at 30°C.

Scanning electron microscopy images were recorded using a FEI Quanta 200F.

The 3D topographies were recorded in tapping mode at a scanning rate of 1 Hz with an atomic force microscope (AFM) MFP 3D Infinity.

Using a microprobe station (Cascade Microtech, PM8), 2-point current-voltage scans were recorded and the (lateral) thin-film conductivity was evaluated from a simple linear fit (Ohm's law). The measurements were performed at room temperature and under ambient atmosphere and the geometry of the channel was 2.5 µm (length) × 10 mm (total width) × 40 nm (height). The data were recorded using a Keithley (2401) sourcemeter by sweeping the voltage from –4 V to 4 V and back (hysteresis scan) at a scan rate of 500 mV s^{-1}. Contact resistance between the Au contacts and the thin film are neglected when using 2-point probe measurements (as opposed to 4-point probe measurements) because the film's conductivity was high enough to neglect this parameter.

Results and Discussion

NiDPP – UV-Vis-NIR spectrophotometry

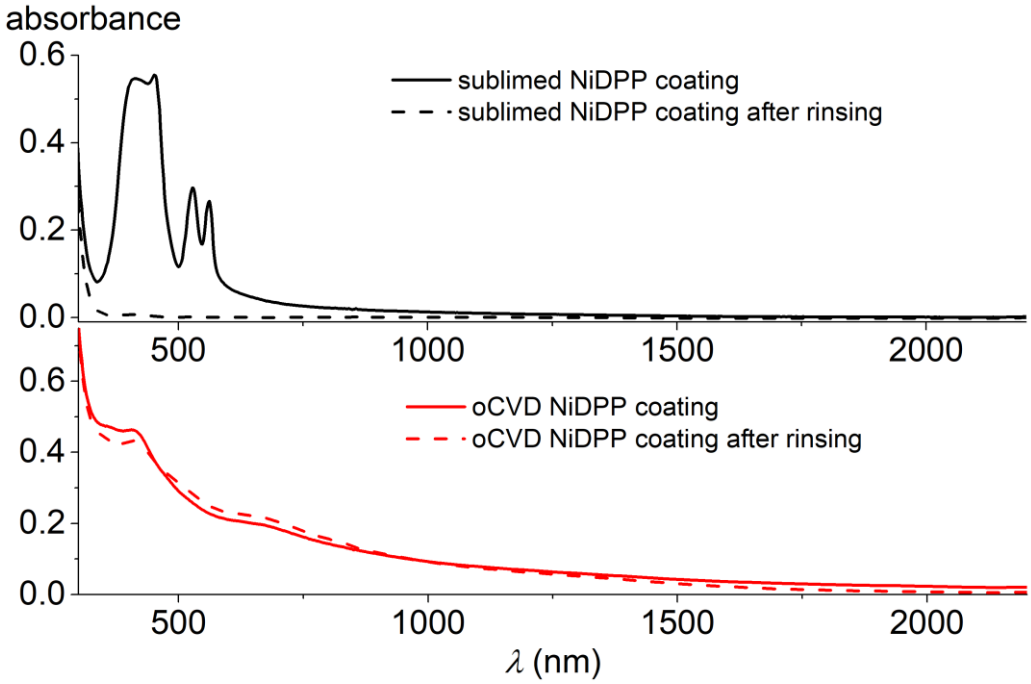

Figure S1. UV-Vis-NIR spectra of as-deposited (solid lines) and acetone rinsed (dashed lines) sublimed NiDPP coating (top) and oCVD NiDPP coating (bottom) on microscope glass slides.

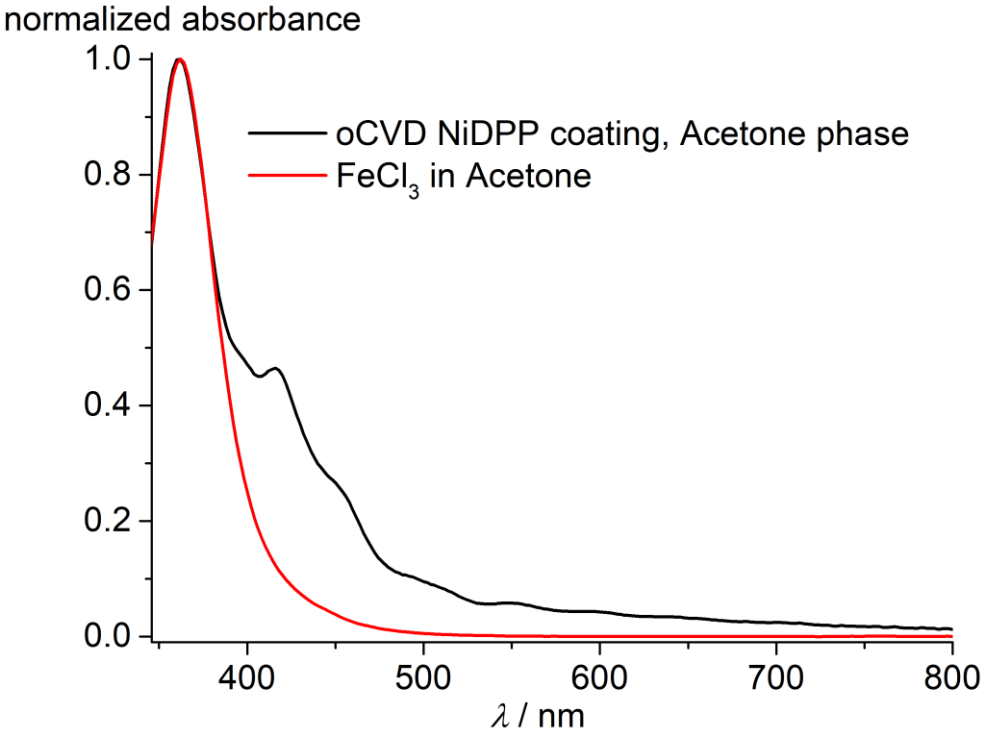

Figure S2. UV-Vis-NIR spectra of the soluble phase of the oCVD NiDPP coating in acetone (black) and its comparison to the spectrum of $FeCl_3$ in acetone (red). The analysis confirms the presence of unreacted $FeCl_3$ in the soluble phase of the oCVD NiDPP coating in acetone.

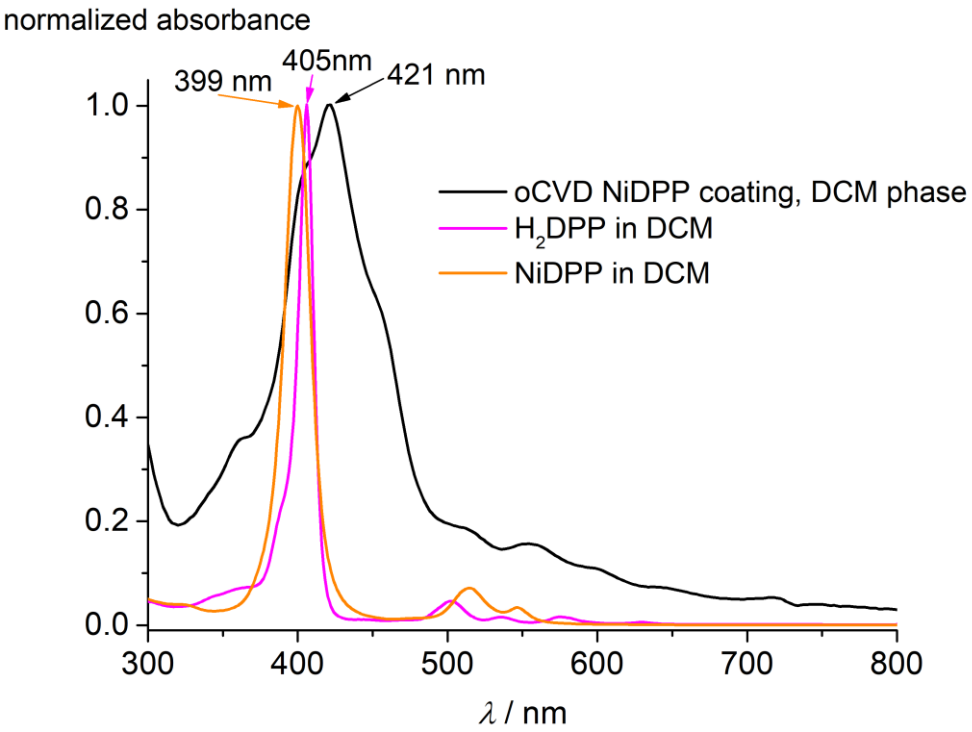

Figure S3. UV-Vis-NIR spectra of the soluble phase of the oCVD NiDPP coating in DCM (black) and its comparison to the spectra of NiDPP (orange) and H_2DPP (pink) in DCM. UV-Vis-NIR spectrum of the soluble phase of oCVD NiDPP coating in DCM exhibits a strong redshift and broadening and a change in the number of Q bands.

NiDPP – X-ray photoelectron spectroscopy

Table S1. Relative atomic concentration of the oCVD NiDPP coating and theoretical composition of NiDPP and fused NiDPP oligomers.

	Ni (%)	N (%)	C (%)	Cl (%)	Fe (%)
oCVD NiDPP coating	2.0	7.7	85.2	2.1	3.0
NiDPP & fused NiDPP oligomers	2.7	10.8	86.5	0.0	0.0

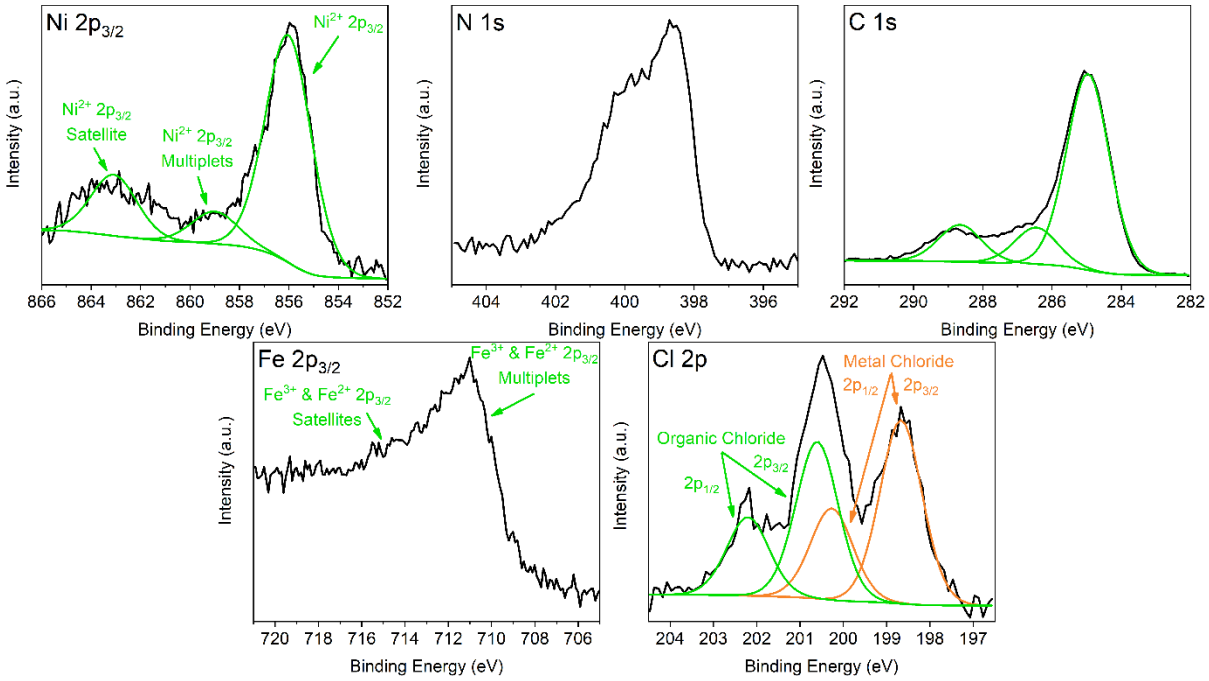

Figure S4. XPS spectra of the Ni $2p_{3/2}$, N 1s, C 1s, Fe $2p_{3/2}$ and Cl 2p core levels of the oCVD NiDPP coating. The binding energy of the main Ni $2p_{3/2}$ core level at 256.0 eV is consistent with the value reported for other nickel(II) porphyrins. Similarly to what observed for other nickel(II) porphyrins, the main Ni $2p_{3/2}$ peak is associated to weaker multiplets at higher binding energies (*ca.* 857.0 to 859.0 eV).[3] Interestingly, the Ni $2p_{3/2}$ XPS spectrum reveals the presence of a shake-up satellite at 863.1 eV, which has been reported for *β*-substituted nickel(II) porphyrins. This observation is consistent with the formation of triply linked *meso-meso*/*β-β*/*β-β* and doubly linked *meso-β*/*meso-β* linkages between the selected di-*meso*-subsituted nickel(II) porphyrin. The N 1s XPS spectrum shows a main peak at 399.1 eV, which is characteristic of the pyrrolic nitrogen in the nickel (II) porphyrins,[3] and a broadening towards higher binding energies that may arise from the multiplicity of bindings that affect the pyrrole rings (*i.e. meso-meso*, *β-β* and *meso-β* as well as chlorination at the *meso* and *β* positions). The C 1s XPS spectrum mainly shows three contributions associated to carbons pertaining to the phenyl rings (284.9 eV) and to the pyrrole rings (286.4 eV) and the pyrrole carbon shake-up transitions (288.6 eV) that is characteristic of porphyrins.[3] The Fe $2p_{3/2}$ reveal a main peak at 711.6 eV that can be attributed to unreacted ferric chloride ($FeCl_3$).[4] A second and poorly resolved contribution spreading around 716.0 eV is observed and associated to satellite peak.[4] The presence of ferrous chloride ($FeCl_2$) cannot be excluded, however, the Fe $2p_{3/2}$ multiplets that spread from 709.8 eV to 711.5 eV for $FeCl_2$ and from 711.3 eV to 714.2 eV for $FeCl_3$ complicate the attribution unreacted products and by-products.[4] Finally, the Cl 2p XPS spectrum reveals the presence of two chlorine environments associated to the metal chloride environment (Cl $2p_{3/2}$ = 198.7 eV and Cl $2p_{1/2}$ = 200.3 eV) related to the presence of unreacted $FeCl_3$ or $FeCl_2$ by-products in the oCVD NiDPP coating, and to organic chloride (Cl $2p_{3/2}$ = 200.6 eV and Cl $2p_{1/2}$ = 202.2 eV) related to the chlorination of the porphyrins.

NiDD*t*-BuPP – UV-Vis-NIR spectrophotometry

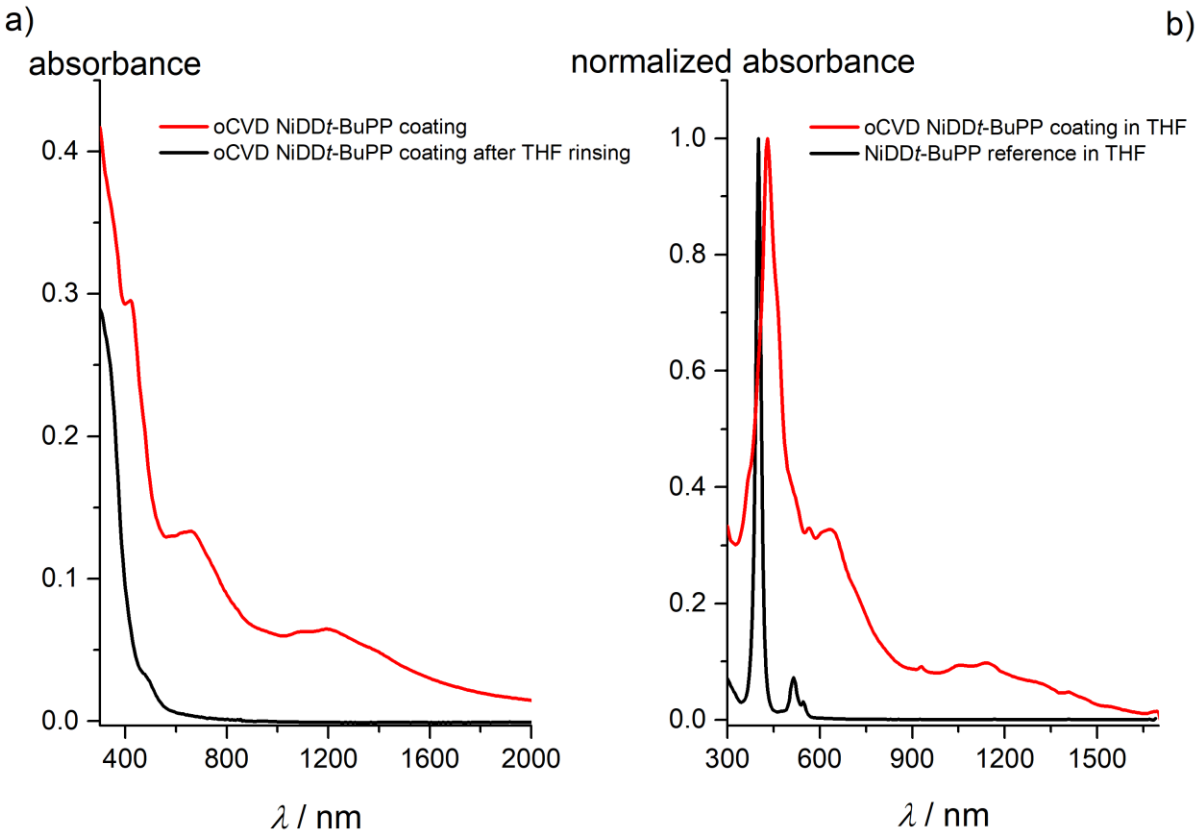

Figure S5. UV-Vis-NIR spectra of a) oCVD NiDD*t*-BuPP coating on glass as-deposited (red) and after rinsing with THF (black), b) the oCVD NiDD*t*-BuPP coating dissolved in THF (red) and NiDD*t*-BuPP monomer in THF (black). The oCVD NiDD*t*-BuPP coating exhibit NIR absorption similarly to the oCVD NiDPP coating. In contrast with the oCVD NiDPP coating, the oCVD NiDD*t*-BuPP coating is fully soluble in THF, exhibiting a strong redshift of the B-bands (30 nm) when compared to the pristine monomer dissolved in THF and a strong NIR absorption which is coherent with the formation of multiply fused porphyrin oligomers.

NiDD*t*-BuPP – Laser desorption ionization high-resolution mass spectrometry

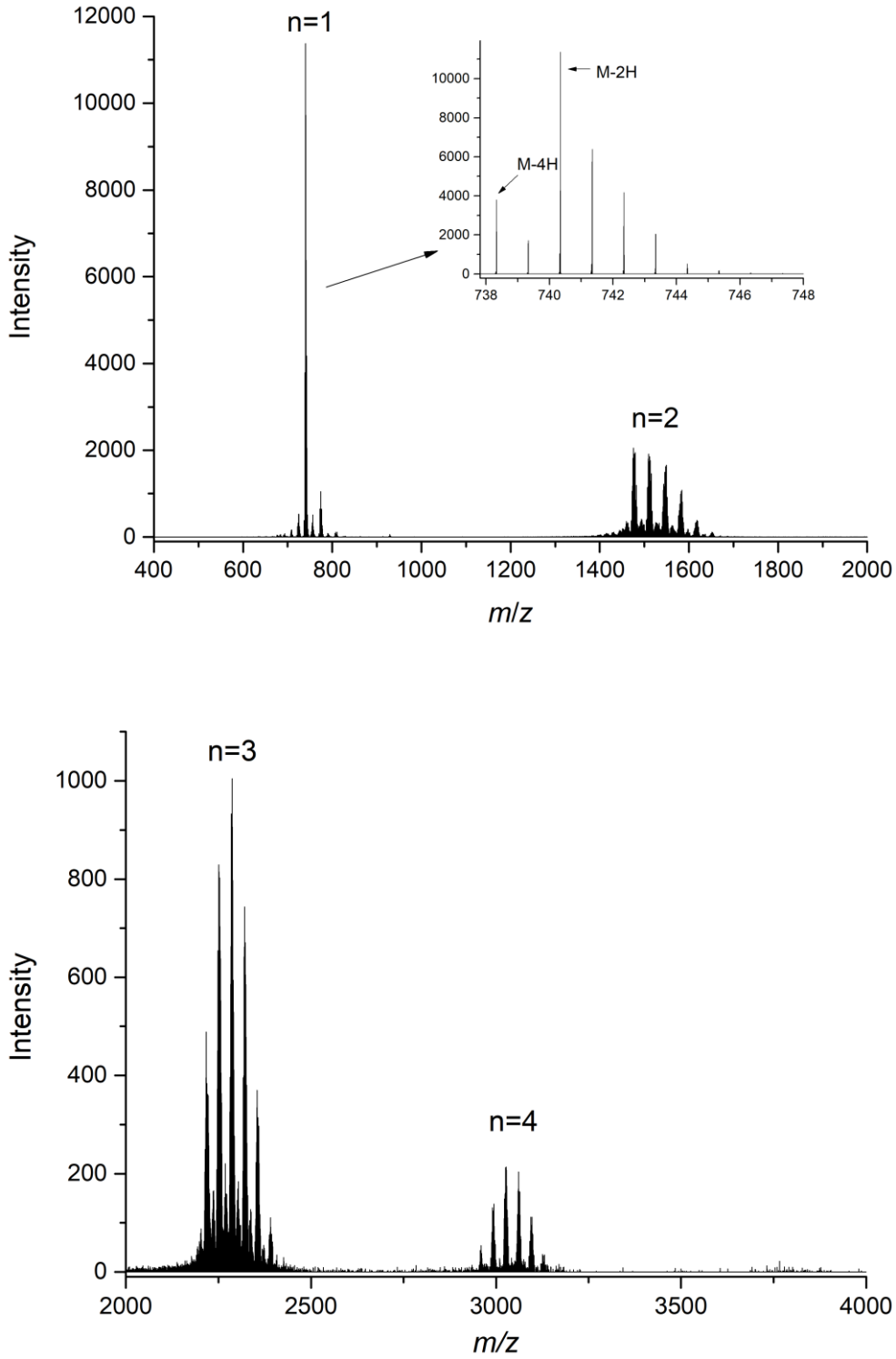

Figure S6. LDI-HRMS spectra of oCVD NiDD*t*-BuPP coating. It evidences the formation of oligomers. Similarly to the mass spectra of the oCVD NiDPP coating, the loss of 2H proportional to the number of phenyl rings is observed (inset). Chlorination of the NiDD*t*-BuPP monomer and P(NiDD*t*-BuPP) oligomers is observed.

NiDD*t*-BuPP – Gel permeation chromatography

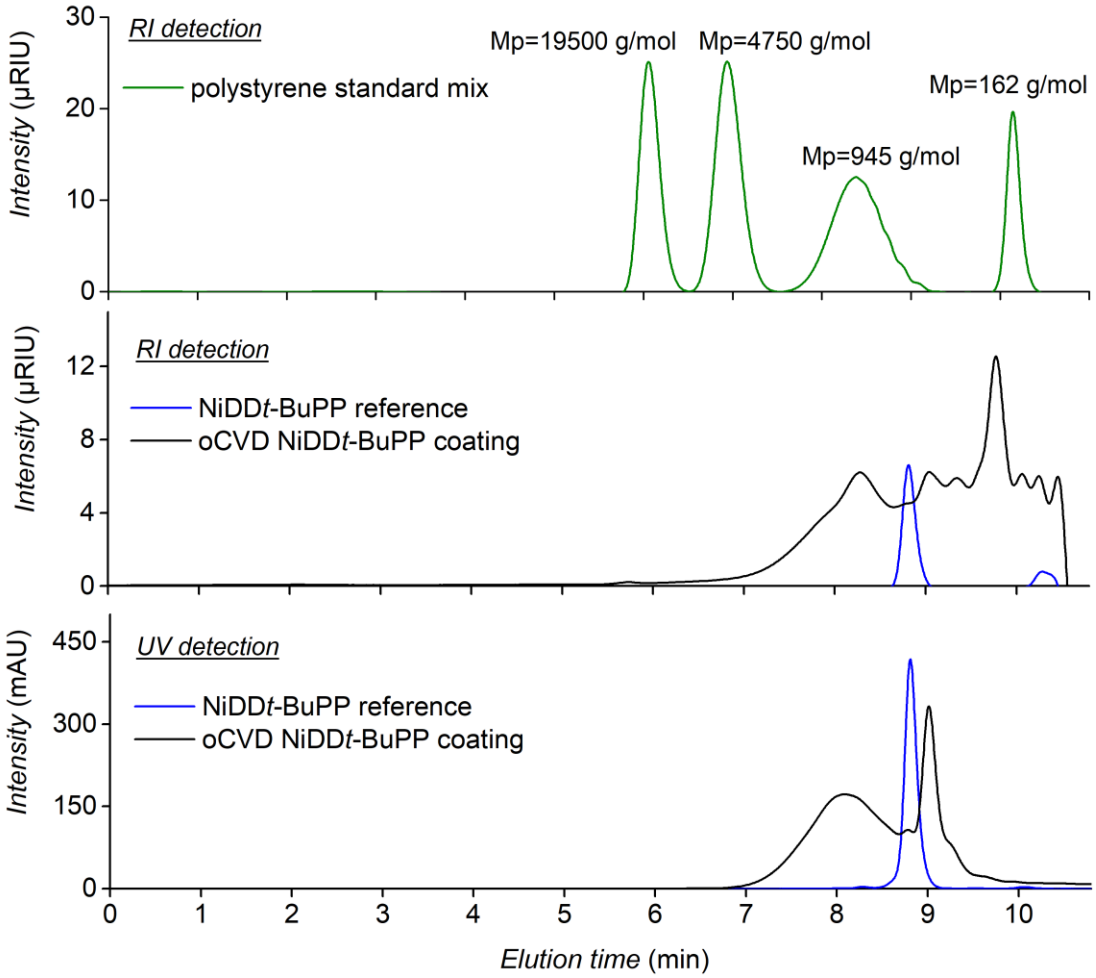

Figure S7. GPC chromatograms of NiDD*t*-BuPP monomer (blue) and its corresponding oCVD NiDD*t*-BuPP coating (black), with RI and UV (@ 430 nm) detection. The chromatogram of the oCVD NiDD*t*-BuPP coating shows a mass distribution up to 5,000 g·mol^{-1} when compared to polystyrene narrow standards. The UV-Vis detection allow the discrimination between the porphyrin-based components and the $FeCl_3$. It has to be noted that the comparison to polystyrene narrow standards yield an underestimation of the molecular weight of the NiDD*t*-BuPP monomer to a mass around 500 g·mol^{-1}, while NiDDt-BuPP has a molecular weight of 743.67 g·mol^{-1}. Interestingly, the GPC analysis highlighted the elution of porphyrinic compounds (evidenced from the UV-Vis detection at 430 nm) at higher retention times compared to the NiDD*t*-BuPP monomer. According to the LDI-HRMS analysis of the oCVD NiDD*t*-BuPP coating that does not reveal the presence of compounds with mass lower than [(NiDD*t*-BuPP) -H_4]$^+$ (Figure S6), the elution of porphyrinic compounds at higher retention times is unlikely to be related to formation of smaller porphyrin units, but might be related to the intramolecular cyclization between the phenyl ring and porphyrinic macrocycle that implies a more planar structure of the porphyrin. The new conformation could increase the interactions between the porphyrin units and the column stationary phase yielding an increase in the elution time despite the very similar hydrodynamic volume.

NiDPP – Laser desorption ionization high-resolution mass spectrometry

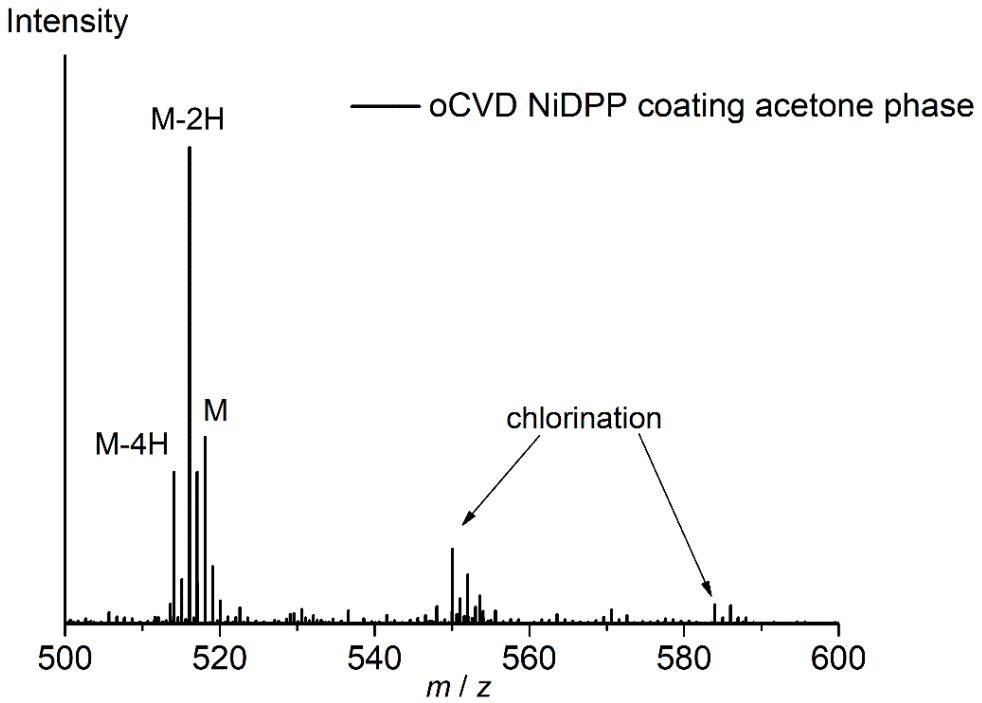

Figure S8. LDI-HRMS spectra of the soluble phase of the oCVD NiDPP coating in acetone. The spectrum displays signals related to the loss of two and four hydrogen atoms (M-2H $C_{32}H_{18}N_4Ni$ 516.088 *m*/z and M-4H $C_{32}H_{16}N_4Ni$ 514.072 *m*/*z*) from the monomer NiDPP. Signals related to the incorporation of one and two chlorine atoms are observed in the higher mass range ($C_{32}H_{17}N_4NiCl$ 550.049 *m*/*z*; $C_{32}H_{15}N_4NiCl$ 548.033 *m*/*z* and $C_{32}H_{16}N_4NiCl_2$ 584.010 *m*/*z*).

NiDD*t*-BuPP – Conductivity measurement

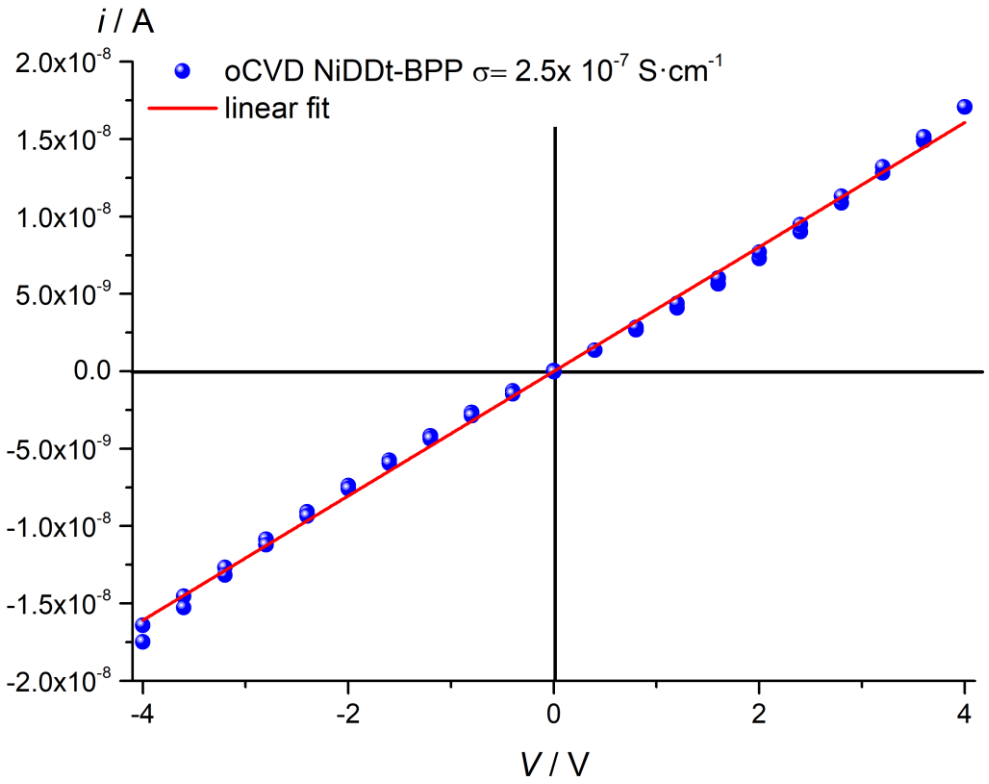

Figure S9. Lateral electrical conductivity measurement for the oCVD NiDD*t*-BuPP coating deposited on an OFET chip used to determine the conductivity. The conductivity measured for the oCVD NiDD*t*-BuPP coating is five orders of magnitude lower compared to the oCVD NiDPP coating.

NiDPP – Scanning electron microscopy and atomic force microscopy

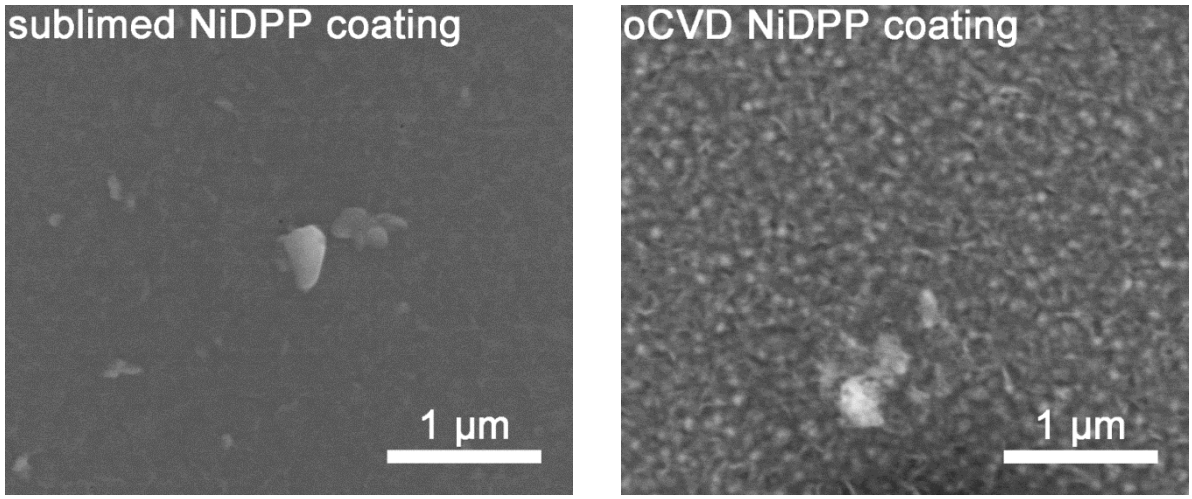

Figure S10. SEM images for the sublimed (left) and oCVD (right) NiDPP coating.

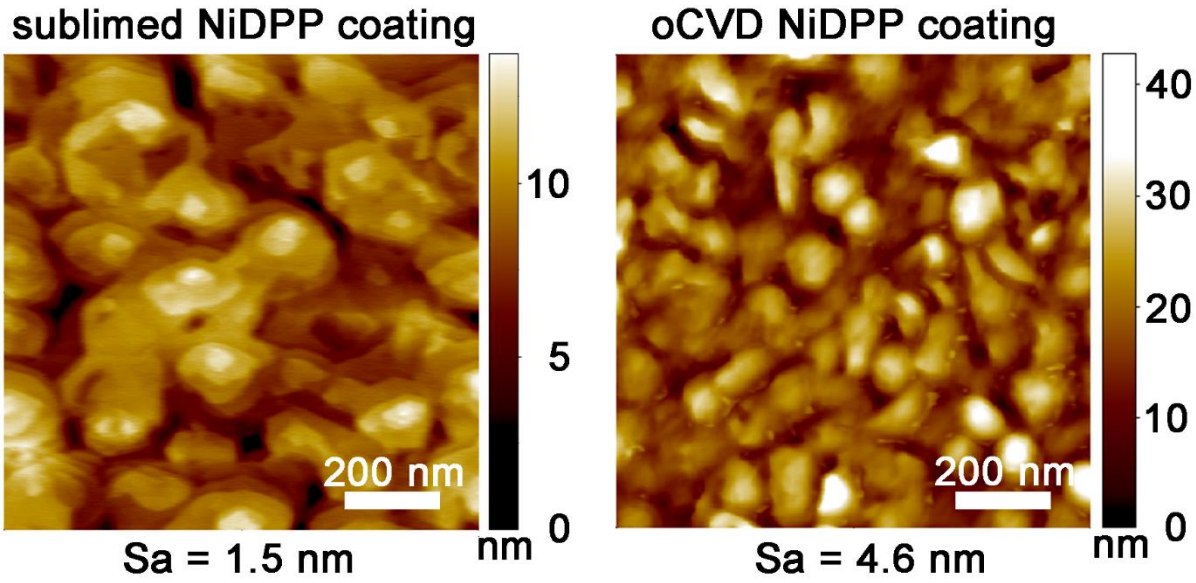

Figure S11. Atomic force microscopy (AFM) images of (left) a 50 nm thick sublimed NiDPP coating and (right) a 200 nm oCVD NiDPP coating deposited on a silicon wafer. The measured average roughnesses (Sa) of the thin films are 1.5 nm and 4.6 nm for the sublimed NiDPP coating and oCVD NiDPP coating, respectively.

References

[1] S. A. Yao, C. B. Hansen, J. F. Berry, *Polyhedron* **2013**, *58*, 2–6.
[2] N. Kamonsutthipaijit, H. L. Anderson, *Chem. Sci.* **2017**, *8*, 2729–2740.
[3] M. Rachele, G. Ricciardi, A. Rosa, *J. Porphyrins Phthalocyanines* **2017**, *21*, 371–380.
[4] A. P. Grosvenor, B. A. Kobe, M. C. Biesinger, N. S. Mcintyre, *Surf. Interface Anal.* **2004**, *36*, 1564–1574.